Dust-Induced Regulation of Thermal Radiation in Water Droplets

Chuan-Xin Zhang(张传新)[1*], Tian-Jiao Li(李天骄)[2], Liu-Jun Xu(须留钧)[3], and Ji-Ping Huang(黄吉平)[1*]

[1]*Department of Physics, State Key Laboratory of Surface Physics, and Key Laboratory of Micro and Nano Photonic Structures (MOE), Fudan University, Shanghai 200438, China*
[2]*MIIT Key Laboratory of Thermal Control of Electronic Equipment, School of Energy and Power Engineering, Nanjing University of Science and Technology, Nanjing 210094, China*
[3]*Graduate School of China Academy of Engineering Physics, Beijing 100193, China*

(Received 11 March 2023; accepted manuscript online 4 April 2023)

Accurate and fast prediction of thermal radiation properties of materials is crucial for their potential applications. However, some models assume that the media are made up of pure water droplets, which do not account for the increasing deviations caused by volcanic eruptions, pollution, and human activities that exacerbate dust production. The distinct radiation properties of water and dust particles make it challenging to determine the thermal radiation properties of water droplets containing dust particles. To address this issue, we investigate the influence of dust particles on light transmission and energy distribution in water droplets using the multiple sphere T-matrix method. By considering different droplet and dust diameters, volume fractions, and position distributions, we analyze how extinction regulation is achieved in dust-containing water droplets. Our results reveal the significant role of dust particles in the thermal radiation effect and provide insights into the electromagnetic properties of colloidal suspensions. Moreover, the dust-induced reestablishment of energy balance raises concerns about environmental management and climate change. This research highlights the importance of accounting for dust particles in atmospheric models and their potential impact on radiative balance.

DOI: 10.1088/0256-307X/40/5/054401

Thermal radiation properties of materials play a crucial role in their potential applications. This is particularly important in understanding cloud formation, as clouds are mainly composed of water droplets that condense around tiny particles of smoke, dust, ash, or salt.[1–4] These droplets determine sunlight transmission and affect cloud generation, lifetime, and radiation. The reaction between water droplets and trace gases also affects the oxidizing power of the atmosphere, the lifetime of greenhouse gas methane, and the concentration of tropospheric ozone.[5–8] The long-term effect of water droplets may lead to significant changes in the greenhouse effect and radiative forcing.

In addition to water droplets, condensation nuclei also affect materials radiation properties.[9–17] These nuclei are generally from soil lifted by the wind, volcanic eruptions, and pollution.[18–21] The different sizes and compositions of dust particles affect water droplet formation, nucleation rate, and water droplet size.[22–24] Since dust particles are small and their properties are difficult to describe precisely, their influence is often ignored.[25–31] However, this assumption has been found to have significant deviations. Coarse dust is significant in climate models, impacting ocean ecosystems, clouds, and global climates.[32–36] It is particularly essential to study the effect of dust particles on radiation properties.

Great research has been conducted on water droplets' radiation properties in clouds and windows. When the water content exceeds 60%, it plays a dominant role in clouds. Humidification enhances particle scattering in the atmosphere.[37,38] The photons scattered to other angles are concentrated in the angular region bounded by the cutoff angles for either external or backside droplets.[39–41] In addition, the contact angle of droplets attached to glasses affects the energy distribution of the receiving surface.[42,43]

Despite much independent research on dust particles or water droplets, investigating water droplets containing dust particles remains challenging due to their distinct physical properties. For example, the black carbon on the surface of water droplets leads to high light absorption. Such absorption enhancement contributes to significant atmospheric heating, which cannot be neglected in aerosol absorption models.[44] Therefore, it is urgent to investigate the influence of dust particles on the radiation properties of water droplets.

To address this critical issue, we establish a computational model and method to describe the influence of dust-containing water droplets on radiation properties. Then, we analyze various parameters for extinction regulation, including the diameters of water droplets and dust particles, the complex refractive indices of dust particles, the position distributions of water droplets in the air, and the concentric and non-concentric dust particles in water droplets. These results provide a general model for understanding the electromagnetic properties of colloidal suspensions.

The amplitude scattering matrix for particles can de-

*Corresponding authors. Email: cxzhang@fudan.edu.cn; jphuang@fudan.edu.cn
© 2023 Chinese Physical Society and IOP Publishing Ltd

scribe the two components of the scattered wave that are parallel and perpendicular to the scattering plane.[45] The amplitude scattering matrix for particles has always been used to describe the relationship between the incident field $(E^{\rm i}_{||},\ E^{\rm i}_{\perp})^{\rm T}$ (the superscript T denotes the transpose of a matrix) and scattered field $(E^{\rm s}_{||},\ E^{\rm s}_{\perp})^{\rm T}$,[46,47]

$$\begin{pmatrix} E^{\rm i}_{||} \\ E^{\rm i}_{\perp} \end{pmatrix} = \frac{\exp(ikr)}{-ikr} \begin{pmatrix} S_2 & S_3 \\ S_4 & S_1 \end{pmatrix} \begin{pmatrix} E^{\rm s}_{||} \\ E^{\rm s}_{\perp} \end{pmatrix}, \quad (1)$$

where the elements S_j $(j = 1, 2, 3, 4)$ of the amplitude scattering matrix depend on scattering angle θ and azimuthal angle ϕ, $i = \sqrt{-1}$, k is the wave vector, and r is the distance between the observation point and particle.

The scattering matrix is dependent on particle size, morphology, composition, and scattering direction, regardless of the specific spatial location. It serves as the fundamental parameter of particle radiation properties, from which other radiation property parameters can be derived. Since the two components of the scattered electric field are difficult to measure directly, the Stokes vector is usually introduced in scattering theory to characterize the intensity and polarization properties of electromagnetic waves.

The Stokes vector is capable of describing the polarization state of light waves through four parameters $[I, Q, U, V]^{\rm T}$. The Stokes vectors of the scattered waves $[I^{\rm s}, Q^{\rm s}, U^{\rm s}, V^{\rm s}]^{\rm T}$ and incident waves $[I^{\rm i}, Q^{\rm i}, U^{\rm i}, V^{\rm i}]^{\rm T}$ are related by a 4×4 amplitude scattering matrix known as the Mueller matrix:[47]

$$\begin{bmatrix} I^{\rm s} \\ Q^{\rm s} \\ U^{\rm s} \\ V^{\rm s} \end{bmatrix} = \frac{1}{k^2 r^2} \begin{bmatrix} S_{11} & S_{12} & S_{13} & S_{14} \\ S_{21} & S_{22} & S_{23} & S_{24} \\ S_{31} & S_{32} & S_{33} & S_{34} \\ S_{41} & S_{42} & S_{43} & S_{44} \end{bmatrix} \begin{bmatrix} I^{\rm i} \\ Q^{\rm i} \\ U^{\rm i} \\ V^{\rm i} \end{bmatrix}. \quad (2)$$

The intensity of the emergent light can be converted from the incoming light by the scattering matrix. In the standard $[I, Q, U, V]^{\rm T}$ representation of polarization, the normalized Stokes scattering matrix has the well-known block-diagonal structure.[48] For independent scattering particles with random orientation distribution and rotational axis symmetry, the dimensionless Stokes scattering matrix can be expressed as

$$\begin{bmatrix} I^{\rm s} \\ Q^{\rm s} \\ U^{\rm s} \\ V^{\rm s} \end{bmatrix} = \begin{bmatrix} S_{11}(\Theta) & S_{21}(\Theta) & 0 & 0 \\ S_{21}(\Theta) & S_{22}(\Theta) & 0 & 0 \\ 0 & 0 & S_{33}(\Theta) & S_{34}(\Theta) \\ 0 & 0 & -S_{34}(\Theta) & S_{44}(\Theta) \end{bmatrix} \begin{bmatrix} I^{\rm i} \\ Q^{\rm i} \\ U^{\rm i} \\ V^{\rm i} \end{bmatrix}, \quad (3)$$

where S is the scattering matrix, and Θ is the scattering angle $(0^\circ < \Theta < 180^\circ)$.

The Mueller matrix contains the intensity and polarization information of the scattered wave, and the scattering phase function Φ of the particle can be obtained from S_{11}[49]

$$\Phi = \frac{4\pi S_{11}}{k^2 C_{\rm sca}}. \quad (4)$$

The scattering phase function Φ describes the distribution of scattered energy in all directions and satisfies the normalization condition. It satisfies the following relationship:[50]

$$\frac{1}{2}\int_0^\pi S_{11}(\Theta)\sin\Theta {\rm d}\Theta = 1. \quad (5)$$

The extinction efficiency and scattering efficiency for spheres are expressed as[51]

$$Q_{\rm ext} = \frac{2}{\chi^2}\sum_{n=1}^{\infty}(2n+1)Re\{a_n + b_n\}, \quad (6)$$

$$Q_{\rm sca} = \frac{2}{\chi^2}\sum_{n=1}^{\infty}(2n+1)[|a_n|^2 + |b_n|^2], \quad (7)$$

where a_n and b_n are the Lorenz–Mie coefficients, $\chi = \pi D/\lambda$ is the size parameter, D is the diameter of spheres, λ is the wavelength. The extinction cross-section $C_{\rm ext}$ and scattering cross-section $C_{\rm sca}$ for spheres are $C_{\rm ext} = (\pi/4)D^2 Q_{\rm ext}$ and $C_{\rm sca} = (\pi/4)D^2 Q_{\rm sca}$, respectively. The degree of linear polarization is $-S_{21}(\Theta)/S_{11}(\Theta)$. The asymmetry parameter describes the ratio of the total scattered energy forward and backward distribution. The asymmetry parameter g reads

$$g = \frac{1}{2}\int_{-1}^{1} S_{11}(\cos\Theta)\cos\Theta {\rm d}\cos\Theta. \quad (8)$$

The value of g is between -1 and 1. A positive value of g indicates that the particle scatters more energy forward, while a negative value indicates more backward scattering energy, and a zero value indicates isotropic scattering. The single scattering albedo is defined as the ratio of the cross-sectional scattering area to the cross-sectional extinction area,

$$\omega = \frac{C_{\rm sca}}{C_{\rm ext}}. \quad (9)$$

The volume-equivalent radius $R_{\rm vol-equ}$ of particles is defined as the sphere radius with the same volume as the target[52]

$$R_{\rm vol-equ} = (N_{\rm s} \times r^3)^{1/3}, \quad (10)$$

where $N_{\rm s}$ is the number of particles, and r is the monomer radius. The linear depolarization ratio, i.e., the ratio of the flux of the cross-polarized component of the backscattered light relative to that of the co-polarized component, can be written as[53–55]

$$\delta_L = \frac{1 - S_{22}/S_{11}}{1 + 2S_{21}/S_{11} + S_{22}/S_{11}}. \quad (11)$$

In lidar and radar remote sensing, the polarization properties of light scattered by particles in the backscattering direction are commonly described in terms of linear and circular depolarization ratios. For spherical particles, both ratios are zero. However, for nonspherical particles, both ratios can significantly deviate from zero and therefore indicate particle nonsphericity. As a result, there has been a growing interest in lidar and radar polarimetry as a remote sensing technique capable of characterizing the shapes of scattering particles. Hence, theoretical and numerical studies of the depolarization ratios are essential and timely.

The superposition T-matrix method is used to generate the scattering and absorption properties of particles,

which are necessary for interpreting the outcomes of remote sensing observations. This method can be applied to particles of various sizes, shapes, and morphologies. To compute the optical properties of non-concentric spherical shell particles, we use the multiple sphere T-matrix code (version 3.0).[56] This code is based on the superposition T-matrix method and can be applied to particles consisting of multiple spheres with non-overlapping surfaces, where the surfaces of any two spheres may share a single point at most. The code uses an iterative method to solve the interaction equation and computes the orientation-averaged optical properties from the T-matrix by using the analytical solution to the integration over Euler angles.[56–58]

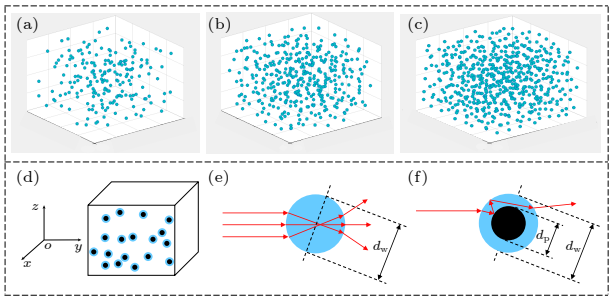

Fig. 1. Effects of water droplets and dust particles on light transmission. The distribution of water droplets with different volume fractions f_v is shown for (a) $f_v = 10\%$, $N_w = 191$, (b) $f_v = 20\%$, $N_w = 382$, and (c) $f_v = 30\%$, $N_w = 573$. (d) Water droplets containing dust particles in a cube with a side length of 20 mm. (e) Light transmission in pure water droplets. (f) Light transmission in water droplets containing dust particles.

A target, as shown in Fig. 1, is characterized by its size parameters, complex refractive indices, and positions relative to a common origin. The description assumes that the spheres are homogeneous and isotropic, although it can be extended to account for layered and optically active spheres. Figures 1(a)–1(c) present the distribution of water droplets with different volume fractions, f_v. The volume fractions of water droplets are 10%, 20%, and 30%, respectively, with corresponding numbers of water droplets, N_w, being 191, 382, and 573, respectively. It is important to note that the spheres in this model cannot overlap.

Figure 1(d) depicts a cube filled with water droplets containing dust particles, randomly distributed throughout the volume. Figures 1(e) and 1(f) show the light transmission in pure droplets and in droplets containing dust, respectively. The diameter of the water droplets, d_w, is fixed at 1 mm, while the diameter of the dust particles, d_p, ranges from 0.02 mm to 0.8 mm. The light's final exit direction is different from that of pure water droplets and is affected by the dust after entering the water droplet. The presence of dust inside the water droplet changes the light direction upon transmission through it.

We calculate the extinction properties of pure water droplets and pure dust particles to illustrate the effect of dust particles on water droplets. The complex refractive index of water droplets, m_w, is set to $1.33 + 0i$. Figure 2(a) shows the extinction efficiency Q_{ext} versus the diameter of water droplets for different numbers. We can observe that the extinction efficiency gradually increases as the droplet diameter increases. Simultaneously, the larger the number of water droplets, the higher the extinction efficiency, as more droplets cause more light to change direction. When the number of droplets remains constant, the larger the droplet diameter, the greater the change in the light direction.[59] Figure 2(b) displays the extinction efficiency versus the volume fraction of water droplets for different diameters. As the volume fraction f_v of water droplets increases, the extinction efficiency gradually increases. Furthermore, for the same volume fraction, the larger the diameter of water droplets, the higher the extinction efficiency. The extinction efficiency positively correlates with the diameter and number of water droplets.

In addition to pure water droplets, we also calculate the extinction properties of pure dust particles. Figures 2(c) and 2(d) show the extinction efficiency versus dust diameter with the complex refractive index for different numbers of pure dust particles. The complex refractive index values m_p of dust particles are $1.57+0i$ and $1.57+0.56i$ in Figs. 2(c) and 2(d), respectively, and the diameters of dust particles d_p are all 2 μm in these two figures. As is seen, in the case of only dust particles, the extinction efficiency gradually increases with the diameter of dust particles. Additionally, the higher the number of dust particles, the greater the extinction efficiency. The imaginary part of the complex refractive index of dust has a significant influence on extinction efficiency. A larger imaginary part will result in higher extinction efficiency.

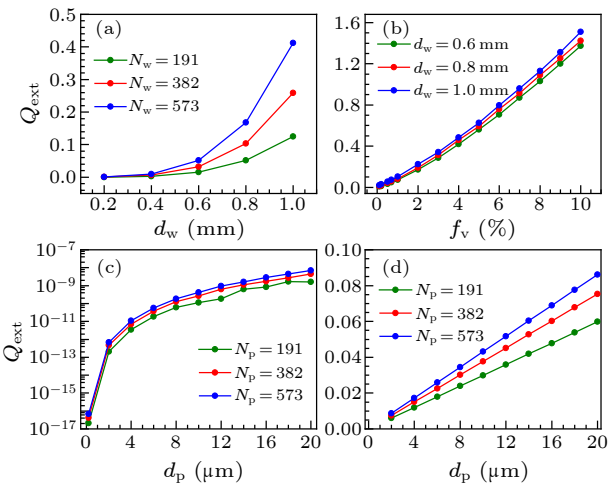

Fig. 2. [(a), (b)] Extinction efficiency of pure water droplets (a) versus droplet diameter d_w for different numbers of N_w, corresponding to $N_w = 191$, 382, and 573, and (b) versus volume fraction f_v of droplets for different diameters of d_w, corresponding to $d_w = 0.6$, 0.8, and 1.0 mm. [(c), (d)] Extinction efficiency of pure dust particles versus dust diameter with complex refractive indices (c) $m_p = 1.57 + 0i$ and (d) $m_p = 1.57 + 0.56i$ for different numbers of particles N_p, corresponding to $N_p = 191$, 382, and 573.

We calculate the extinction properties of water droplets with dust particles. Figure 3(a) displays the extinction efficiency versus the volume fraction of water droplets for different diameters of dust particles. The com-

plex refractive indices of water droplets $m_{\rm w}$ and dust particles $m_{\rm p}$ are $1.33+0i$ and $1.57+0.56i$, respectively. The diameter of water droplets $d_{\rm w}$ is 1.0 mm, and the diameters of dust particles $d_{\rm p}$ range from 0.02 to 0.8 mm.

We observe that the extinction efficiency gradually grows with the increase in the volume fraction of dust particles when $d_{\rm p}$ ranges from 0.02 to 0.8 mm. However, when $d_{\rm p}$ is less than 0.2 mm, the extinction efficiency is inapparent with the increase in dust diameter. Conversely, when $d_{\rm p}$ is more than 0.2 mm, the extinction efficiency shows a significant growth with the increase of $d_{\rm p}$. This is because larger dust particle diameters have a more significant impact on energy distribution, leading to a higher variation in the direction of light.

We accordingly introduce the relative error of the calculated extinction efficiency without considering dust particles to demonstrate the significant effect of dust particles. The relative error of the calculated extinction efficiency without considering dust particles is defined as

$$\delta_{\rm dust} = \frac{|Q_{\rm with} - Q_{\rm without}|}{Q_{\rm with}} \times 100\%, \tag{12}$$

where $Q_{\rm with}$ and $Q_{\rm without}$ are the extinction efficiency of water droplets with dust particles and without dust particles, respectively. Figure 3(b) displays the relative error versus the volume fraction of droplets for different diameters of dust particles. The relative error of the extinction efficiency without considering dust particles increases with the diameter. When the dust particle diameter is 0.4 mm, the relative error is above 26.76%, and the maximum value is up to 69.22%. When the particle diameter is 0.8 mm, the relative error of the extinction efficiency is above 69.51%, and the maximum value is up to 94.50%. These results indicate that larger inclusions have a significant and non-negligible extinction effect on water droplets.

Figures 3(c) and 3(d) depict the extinction efficiency and relative error versus volume fraction for different water droplet diameters with a fixed dust particle diameter of 0.6 mm. When the water droplet diameter is 0.8 mm, the relative error of the extinction efficiency exceeds 54.81%, with a maximum value of up to 92.87%. Similarly, when the water droplet diameter is 1.0 mm, the relative error of the extinction efficiency is above 52.99%, with a maximum value of up to 88.25%. Smaller water droplet diameters result in more significant extinction efficiency due to their higher quantity. The relative error of extinction efficiency without considering dust particles is calculated using Eq. (13). As the water droplet diameter decreases, the relative error increases.

In Fig. 3(e), we present the extinction efficiency versus the volume fraction of water droplets for different complex refractive indices of dust particles. The diameters of water droplets $d_{\rm w}$ and dust particles $d_{\rm p}$ are 1 mm and 0.6 mm, respectively. We observe that the imaginary part of the complex refractive index of dust particles, which represents the extinction part of light, has a more significant impact on extinction efficiency by comparing the blue and green parts in the figure. The real part of the complex refractive index of dust, which represents the deflection of light, has less influence on extinction efficiency by comparing the blue and red parts in the figure. The gap between the data sets gradually grows as the volume fraction increases.

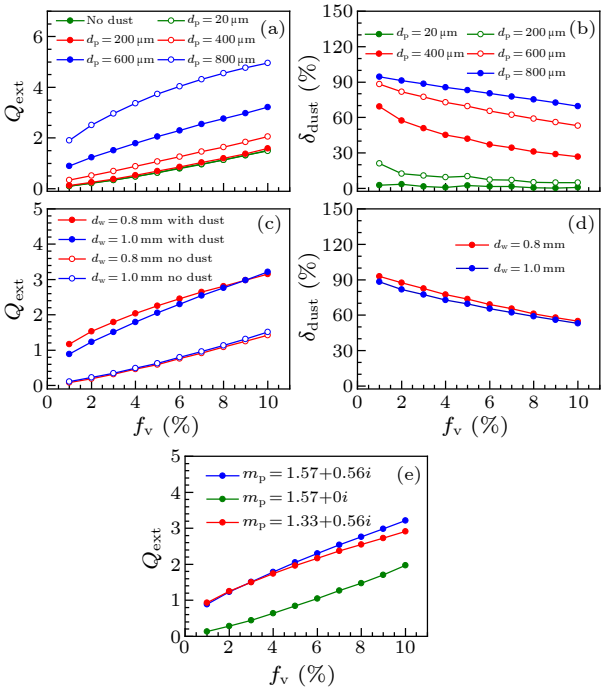

Fig. 3. Effects of diameter and complex refractive index on extinction efficiency. (a) Extinction efficiency versus volume fraction of water droplets, and (b) relative error versus volume fraction of water droplets for different diameters of dust particles $d_{\rm p}$, corresponding to $d_{\rm p}$ = 0.02, 0.2, 0.4, 0.6, and 0.8 mm. (c) Extinction efficiency versus volume fraction of water droplets, and (d) relative error versus volume fraction of water droplets for different diameters of water droplets $d_{\rm w}$, corresponding to $d_{\rm w}$ = 0.8 and 1.0 mm. (e) Extinction efficiency versus volume fraction of water droplets for different complex refractive index values of dust particles $m_{\rm p}$, corresponding to $m_{\rm p} = 1.57+0.56i$, $1.57+0i$, and $1.33+0.56i$.

Next, we discuss the effects of the position distribution of droplets and dust particles. We assume that the diameter of droplets $d_{\rm w}$ is 1.0 mm, and the diameters of dust particles $d_{\rm p}$ are 0.02 and 0.6 mm, respectively. Figure 4(a) reflects the extinction efficiency versus the volume fraction for different position distributions of droplets. Note that water droplets are randomly distributed in the cube. The relative error of extinction efficiency when the water droplets are located differently is defined as follows:

$$\delta_{\rm distribution} = \frac{|Q_{\rm distribution,A} - Q_{\rm distribution,B}|}{Q_{\rm distribution,A}} \times 100\%, \tag{13}$$

where $Q_{\rm distribution,A}$ and $Q_{\rm distribution,B}$ are the extinction efficiencies for position distributions A and B of droplets, respectively. Figure 4(b) displays the relative error versus volume fraction of droplets for different positions of droplets. Our findings suggest that the position distribution of droplets has a negligible effect on extinction efficiency, with relative errors up to 4.86% and 1.32% for $d_{\rm p}$ = 0.02 and 0.6 mm, respectively. The smaller the

diameter of the dust particles, the greater the effect of the droplet position distribution on extinction efficiency. When the number of water droplets is constant, smaller dust particles are more susceptible to position distribution, leading to a greater impact on their corresponding results and making them more sensitive to changes in distribution. However, when the volume fraction of droplets is the same, the position distribution barely affects extinction efficiency, as shown in the figure.

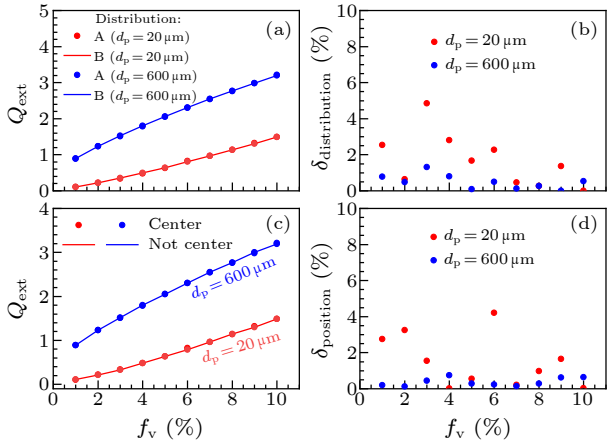

Fig. 4. Effects of position distribution on extinction efficiency. (a) Extinction efficiency versus volume fraction of droplets, and (b) relative error versus volume fraction of droplets for different positions of droplets, corresponding to distributions A and B. (c) Extinction efficiency versus volume fraction of droplets, and (d) relative error versus volume fraction of droplets for different dust positions in droplets, corresponding to dust particles at the center and not at the center of droplets. The complex refractive index of water droplets m_w and dust particles m_p are $1.33 + 0i$ and $1.57 + 0.56i$, respectively.

Figures 4(c) and 4(d) present the extinction efficiency versus volume fraction of droplets and the relative error versus volume fraction of droplets for different dust positions in droplets. The relative error of extinction efficiency when the dust location is different is calculated as follows:

$$\delta_{\text{position}} = \frac{|Q_{\text{center}} - Q_{\text{notcenter}}|}{Q_{\text{center}}} \times 100\%, \qquad (14)$$

where Q_{center} and $Q_{\text{notcenter}}$ represent the extinction efficiency for concentric and non-concentric dust in droplets, respectively.

The position of dust in droplets has a minor impact on the extinction efficiency, with relative errors reaching up to 4.22% and 0.75% for $d_p = 0.02$ and 0.6 mm, respectively. The calculation results are similar no matter whether the dust is located in the center of the water droplet. The relative error does not exceed 4.22% at most, and the larger the dust diameter, the smaller the relative error. It can be observed from the figure that, when the volume fraction is the same, the position of a dust particle in droplets has little effect on extinction efficiency.

In summary, we have examined the impact of dust on the regulation of thermal radiation in water droplets, with a specific focus on various factors such as the complex refractive index of dust, the diameters of both dust and water droplets, and the position distribution of dust and water droplets on the extinction coefficient of dust-containing water droplets. Our research findings offer valuable insights into the electromagnetic properties of colloidal suspensions, which can be extended to compute the radiation properties of impurity-containing liquids. Moreover, our study contributes to better understanding the influence of dust particles on environmental management and addressing climate change.

Acknowledgments. This work was supported by the National Natural Science Foundation of China (Grant No. 12035004), and the Science and Technology Commission of Shanghai Municipality (Grant No. 20JC1414700). We thank Dr. Daniel Mackowski and Dr. Michael Mishchenko for providing the multiple sphere T-matrix code.

References

[1] Kelly J T, Chuang C C, and Wexler A S 2007 *Atmos. Environ.* **41** 2904
[2] Karydis V A, Kumar P, Barahona D, Sokolik I N, and Nenes A 2011 *J. Geophys. Res.* **116** D23204
[3] Karydis V A, Tsimpidi A P, Bacer S, Pozzer A, Nenes A, and Lelieveld J 2017 *Atmos. Chem. Phys.* **17** 5601
[4] Gaston C J 2020 *Acc. Chem. Res.* **53** 1005
[5] Li Y Y, Zhou Y X, Marchesoni F, and Ghosh P K 2022 *Soft Matter* **18** 4778
[6] Huang J P 2020 *Theoretical Thermotics: Transformation Thermotics and Extended Theories for Thermal Metamaterials* (Singapore: Springer) p 231
[7] Xu L J and Huang J P 2023 *Transformation Thermotics and Extended Theories: Inside and Outside Metamaterials* (Singapore: Springer) p 9
[8] Yang S, Wang J, Dai G L, Yang F B, and Huang J P 2021 *Phys. Rep.* **908** 1
[9] Tobo Y, Zhang D, Matsuki A, and Iwasaka Y 2010 *Proc. Natl. Acad. Sci. USA* **107** 17905
[10] Lee K, Lee K I, Jeon S Y, and Kim S 2019 *Adv. Powder Technol.* **30** 190
[11] Boje A and Kraft M 2022 *J. Aerosol Sci.* **159** 105895
[12] Fan C Z, Gao Y, and Huang J P 2008 *Appl. Phys. Lett.* **92** 251907
[13] Li Y, Shen X Y, Wu Z H, Huang J Y, Chen Y X, Ni Y S, and Huang J P 2015 *Phys. Rev. Lett.* **115** 195503
[14] Xu L J, Xu G Q, Huang J P, and Qiu C W 2022 *Phys. Rev. Lett.* **128** 145901
[15] Xu L J, Xu G Q, Li J X, Li Y, Huang J P, and Qiu C W 2022 *Phys. Rev. Lett.* **129** 155901
[16] Jin P, Liu J R, Xu L J, Wang J, Ouyang X P, Jiang J H, and Huang J P 2023 *Proc. Natl. Acad. Sci. USA* **120** e2217068120
[17] Zhang Z R, Xu L J, Qu T, Lei M, Lin Z K, Ouyang X P, Jiang J H, and Huang J P 2023 *Nat. Rev. Phys.* **5** 218
[18] Abubakar A A, Yilbas B S, Hussain A Q, Hassan G, and Adukwu J E 2021 *Sci. Rep.* **11** 18361
[19] Xu L J and Huang J P 2020 *Chin. Phys. Lett.* **37** 080502
[20] Xu L J and Huang J P 2020 *Chin. Phys. Lett.* **37** 120501
[21] Zhang Z R and Huang J P 2022 *Chin. Phys. Lett.* **39** 075201
[22] Wang W J, Liu W, Qi T T, Qiu W Q, Jia H Y, Wang Y J, Shen J, Liu Z, and Thomas J C 2020 *Powder Technol.* **366** 546
[23] Galogahi F M, Zhu Y, An H, and Nguyen N T 2021 *Microfluid Nanofluid* **25** 82
[24] Yu Y, Wu Q, Wang X W, and Yang X B 2012 *Chin. Phys. Lett.* **29** 026802
[25] Wu Y, Cheng T, Gu X, Zheng L, Chen H, and Xu H 2014 *J. Quant. Spectrosc. Radiat. Transfer* **135** 9

[26] Tuzet F, Dumont M, Arnaud L, Voisin D, Lamare M, Larue F, Revuelto J, and Picard G 2019 *Cryosphere* **13** 2169
[27] Zheng L J and Wu Y 2021 *J. Quant. Spectrosc. Radiat. Transfer* **258** 107388
[28] Dang S, Brady J, Rel R, Surineni S, O'Shaughnessy C, and McGorty R 2021 *Soft Matter* **17** 8300
[29] Fedoseev A V, Salnikov M V, Vasiliev M M, and Petrov O F 2022 *Phys. Rev. E* **106** 025204
[30] Ouyang Y L, Zhang Z W, Yu QC, He J, Yan G, and Chen J 2020 *Chin. Phys. Lett.* **37** 126301
[31] Yan S S, Wang Y, Gao Z B, Long Y, and Ren J 2021 *Chin. Phys. Lett.* **38** 27301
[32] Adebiyi A A and Kok J F 2020 *Sci. Adv.* **6** eaaz9507
[33] Kushnir D, Ruscher C, Bartsch E, Thalmann F, and Hébraud P 2022 *Phys. Rev. E* **106** 034611
[34] Li T J, Gao P, Zhang C X, Yuan Y, Liu D, Shuai Y, and Tan H P 2022 *Opt. Lasers Eng.* **158** 107159
[35] Wang C H, Liu Z Y, Jiang Z Y, and Zhang X X 2022 *Phys. Fluids* **34** 062012
[36] Li H R, Wang S M, Wang X Z, Niu X J, and Li Y 2022 *Desalination* **538** 115897
[37] Wagner R, Benz S, Möhler O, Saathoff H, Schnaiter M, and Schurath U 2005 *J. Phys. Chem. A* **109** 7099
[38] Wang X, Niu C, Qi H, and Ruan L 2011 *Procedia Environ. Sci.* **11** 1493
[39] Huang Y, Feng C, Hoeniges J, Zhu K, and Pilon L 2020 *J. Quant. Spectrosc. Radiat. Transfer* **251** 107039
[40] Hoeniges J, Zhu K, Welch W, Simsek E, and Pilon L 2021 *J. Quant. Spectrosc. Radiat. Transfer* **275** 107876
[41] Simsek E, Williams M J, Hoeniges J, Zhu K, and Pilon L 2022 *Int. J. Heat Mass Transfer* **194** 123043
[42] Zhang C, Li T, Yuan Y, Wang F, and Tan H 2020 *Opt. Laser Eng.* **128** 106044
[43] Zhang C, Shi X, Li T, Yuan Y, Wang F, and Tan H 2020 *J. Quant. Spectrosc. Radiat. Transfer* **245** 106856
[44] Zhang Q and Thompson J E 2015 *J. Atmos. Sol.-Terr. Phys.* **133** 121
[45] Yang P, Gao B C, Wiscombe W J, Mishchenko M I, Platnick S E, Huang H L, Baum B A, Hu Y X, Winker D M, Tsay S C, and Park S K 2002 *Appl. Opt.* **41** 2740
[46] Mishchenko M I 2007 *Opt. Express* **15** 13188
[47] Bohren C F and Huffman D R 1998 *Absorption and Scattering of Light by Small Particles* (New York: John Wiley & Sons) p 1
[48] Mishchenko M I, Liu L, Travis L D, and Lacis A A 2004 *J. Quant. Spectrosc. Radiat. Transfer* **88** 139
[49] Modest M F 2013 *Radiative Heat Transfer* 3rd edn (New York: Academic Press) p 1
[50] Wu Y, Cheng T, Zheng L, and Chen H 2017 *J. Quant. Spectrosc. Radiat. Transfer* **195** 147
[51] Mishchenko M I, Videen G, and Yang P 2017 *Opt. Lett.* **42** 4873
[52] Wu Y, Cheng T, Zheng L, and Chen H 2016 *J. Quant. Spectrosc. Radiat. Transfer* **179** 139
[53] Mishchenko M I and Hovenier J W 1995 *Opt. Lett.* **20** 1356
[54] Kahnert M, Kanngießer F, Järvinen E, and Schnaiter M 2020 *J. Quant. Spectrosc. Radiat. Transfer* **254** 107177
[55] Muñoz O, Frattin E, Jardiel T, Gómez-Martín J C, Moreno F, Ramos J L, Guirado D, Peiteado M, Caballero A C, Milli J, and Ménard F 2021 *Astrophys. J. Suppl. Ser.* **256** 17
[56] Mackowski D W and Mishchenko M I 2011 *J. Quant. Spectrosc. Radiat. Transfer* **112** 2182
[57] Kanngießer F, Kahnert M, and Kahnert M 2021 *Opt. Express* **29** 34926
[58] Mishchenko M I 2009 *J. Quant. Spectrosc. Radiat. Transfer* **110** 1210
[59] Liu L H, Tan H P, and Tong T W 2002 *J. Quant. Spectrosc. Radiat. Transfer* **72** 747